Three-dimensional roughness of stylolites in limestones

François Renard,[1,2] Jean Schmittbuhl,[3] Jean-Pierre Gratier,[1] Paul Meakin,[2,4] and Enrique Merino[5]

Received 25 April 2003; revised 28 January 2004; accepted 5 February 2004; published 27 March 2004.

[1] Stylolites are dynamic roughly planar surfaces formed by pressure solution of blocks of rocks into each other. The three-dimensional geometry of 12 bedding-parallel stylolites in several limestones was measured using laser and mechanical profilometers, and statistical characteristics of the surfaces were calculated. All the stylolites analyzed turn out to have self-affine fractal roughness with a well-characterized crossover length scale separating two self-affine regimes. Strikingly, this characteristic length scale falls within a very narrow range for all the stylolites studied, regardless of the microstructure sizes. To explain the data, we propose a continuous phenomenological model that accounts for the development of the measured roughness from an initially flat surface. The model postulates that the complex interface morphology is the result of competition between the long-range elastic redistribution of local stress fluctuations, which roughen the surface, and surface tension forces along the interface, which smooth it. The model accounts for the geometrical variability of stylolite surfaces and predicts the dependence of the crossover length scale on the mechanical properties of the rock. *INDEX TERMS:* 3902 Mineral Physics: Creep and deformation; 3909 Mineral Physics: Elasticity and anelasticity; 3947 Mineral Physics: Surfaces and interfaces; 3675 Mineralogy and Petrology: Sedimentary petrology; 5112 Physical Properties of Rocks: Microstructure; *KEYWORDS:* stylolite, surface roughness, elasticity, surface tension

Citation: Renard, F., J. Schmittbuhl, J.-P. Gratier, P. Meakin, and E. Merino (2004), Three-dimensional roughness of stylolites in limestones, *J. Geophys. Res.*, *109*, B03209, doi:10.1029/2003JB002555.

1. Introduction

[2] Stylolites are partings between blocks of rock which exhibit complex mutual column-and-socket interdigitation [see *Dunnington*, 1967, p. 340]. They are planar, extend laterally for up to tens of meters, may cut across bedding, and often occur in sets, in carbonate and other essentially monomineralic rocks. They play an important role in compaction and creep processes [*Bathurst*, 1971], and therefore in the rheological properties of the upper crust.

[3] The works of *Stockdale* [1922], *Dunnington* [1954, 1967], *Heald* [1959], *Park and Schot* [1968], *Arthaud and Mattauer* [1969], *Guzzetta* [1984], *Dewers and Ortoleva* [1990], *Carrio-Schaffhauser et al.* [1990], and many more leave little doubt that stylolites are the planar, disk-like seams left by self-localized pressure solution that *Fletcher and Pollard* [1981] viewed as ''anticracks''. So much rock may be pressure-dissolved during stylolites formation that stylolitization may considerably change the shape and reduce the thickness of a sedimentary body [*Dunnington*, 1967; *Bathurst*, 1971]. Stylolites seams are often highlighted by a thin concentration of darker material, usually assumed to be insoluble material but at least in some cases shown to be authigenic [*Merino et al.*, 1983; *Thomas et al.*, 1993]. Cataclastic deformation and microtransform faulting contribute to the specific shape of the column and sockets interdigitations [*Deelman*, 1976; *Dickinson and Milliken*, 1995; *Merino and Wang*, 2001].

[4] *Bayly* [1986] attempted to account for the topography of stylolites by invoking a non-uniform distribution of clay particles in the carbonate rock and water flow parallel to the stylolitic plane, but the stylolitic surfaces he predicted apparently have a ridge-and-groove morphology rather than the observed column-and-socket form. *Gal et al.* [1998] carried out a stability analysis for a stressed pressure-solution surface, which was assumed to be free, on which a sinusoidal perturbation is imposed. They concluded that the competition between surface tension and elastic strain energy may render the surface unstable to the growth of perturbations of certain wavelengths and may account for the formation of the roughness of stylolites. This is a stress-dissolution instability, known to physicists as the Asaro-Tiller-Grinfeld instability [*Asaro and Tiller*, 1972; *Grinfeld*, 1986; *Nozieres*, 1995; *Kassner et al.*, 2001]. In another paper [*Gal and Nur*, 1998], they explained why stylolites form by dissolving more on one side than on the other. The local variations in elastic strain energy can induce a small asymmetry of the dissolution front that tends to grow with time.

[5] The usual way of studying stylolites is by examining them in two-dimensional polished cross-sections perpendic-

[1]Laboratoire de Géophysique Interne et Tectonophysique, Université Joseph Fourier, Grenoble, France.
[2]Physics of Geological Processes, University of Oslo, Oslo, Norway.
[3]Ecole Normale Supérieure, Laboratoire de Géologie, Paris, France.
[4]Idaho National Engineering and Environmental Laboratory, Idaho Falls, Idaho, USA.
[5]Department of Geological Sciences, Indiana University, Bloomington, Indiana, USA.

0148-0227/04/2003JB002555$09.00

Table 1. Stylolite Surfaces Analyzed[a]

Stylolite	Origin	Rock	dx, μm	A_{rms}, mm	Length Scale a^*, mm
S0-8	Jura mountains	light yellow limestone	125	0.54	0.77
S1sup	Chartreuse mountains	gray limestone	125	1.48	*
S32	Chartreuse mountains	yellow limestone	125	0.87	*
S3B	Chartreuse mountains	yellow limestone	125	2.32	0.18
S6	Chartreuse mountains	gray limestone	125	1.56	*
S11B	Burgungy	clastic limestone	30	2.49	0.62
S11C	Burgungy	clastic limestone	30	1.68	0.6
S12A	Vercors Mountains	light gray limestone	80	2.86	2.24
S13A	Burgundy	pink-red limestone	30	0.26	0.47
S15A	Burgundy	yellow-red limestone	60	0.61	0.43
S10A	Burgundy	limestone	30	0.83	0.43
Sjuras1	Jura mountains	light yellow limestone	60	0.90	0.96

[a]The resolution in the plane of the stylolite dx, the root mean square roughness (A_{rms}), and the characteristic length a^* are given. An asterisk in the right-hand column indicates a surface with noisy laser data, which was not quantitatively analyzed.

ular to the plane of the stylolite [*Smith*, 2000; *Karcz and Scholz*, 2003]. *Smith* [2000] has studied a three-dimensional image of a stylolite using a series of parallel cross-sections perpendicular to the plane of the stylolite. However, only 20 cross-sections spaced by about 0.5 mm were used, and this is not sufficient to construct a high resolution three-dimensional "map" of the surface.

[6] The objective of the work described in this paper is to quantify the intricate three-dimensional topography of such stylolites. For this purpose we collected twelve sedimentary bed-parallel stylolites in limestones. For all of them, we managed to separate the two interdigitated rock bodies without damaging the peaks, from carefully sawed 20 × 20 × 10 cm blocks of limestones. Thus the full three-dimensional structure of the stylolite interface was revealed, and we quantified their exposed topography using optical and mechanical profilometers. In addition we propose a phenomenological model for surface growth and roughening that reproduces the statistical properties of stylolite surfaces.

2. Analysis of the Stylolites

2.1. Origin and Chemical Characterization of the Stylolites

[7] Decimeter-scale limestone samples from the Chartreuse, Vercors, and Jura mountains and the Burgundy area (France) that have undergone stylolitization were collected in newly open quarries (see Table 1). The age of the limestones varied between Jurassic and Miocene. We selected stylolites that could be separated to reveal the two complementary rough surfaces; see Figures 1 and 2.

[8] Thin sections show that the limestones are recrystallized and that the grain size is below the resolution of the optical microscope. For each stylolite we analyzed two kinds of sample by X-ray fluorescence; the rock itself and the insoluble particles (mainly clays) trapped within the interface. The stylolite interfaces were washed with distilled water and the clay suspensions were collected directly from the solution after filtration, evaporation and drying at 70°C. A small volume in each sample was cut and these rock samples were crushed and sieved. Then all the samples were heated at 1200°C, to remove organic matter, before lithium borate pellets were produced for X-ray fluorescence analysis.

[9] The analysis indicated that the stylolites are enriched in aluminum, iron, titanium, and phosphorus compared with the bulk rock (see Table 2), whereas the interface is depleted in calcium indicating preferential dissolution along the stylolite. However, the concentration ratios between elements are not conserved in the stylolite and in the rock. This may have several explanations, including the following:

[10] 1. The analyzed elements may be shared by a number minerals that have different solubilities. This is commonly associated with pressure solution cleavage differentiation [*Gratier et al.*, 2003].

[11] 2. The stylolites may have nucleated on preexisting surfaces, e.g., a clay seam, that had a different composition from the ambient.

[12] 3. A fluid may have percolated along the stylolites and removed some elements as dissolved or colloidal solids. This is consistent with the analysis of authigenic muscovite in stylolites by *Thomas et al.* [1993].

[13] To estimate the extent of dissolution, we selected the elements associated with minerals that have the smallest solubilities, and were therefore least influenced by the circulating fluid. The concentration ratios of such elements between the stylolite interfacial material and the bulk rock provides a qualitative indication of the amount of dissolution that has occurred. The stylolite interface residues are 5 to 20 times more concentrated in Ti, Fe, and P than the bulk limestone (see Figure 3). Since the interface is 0.5 to 5 mm thick, the thickness of the layer of limestone that has dissolved is estimated to lie in the range 2.5 to 100 mm. This value is comparable with the maximum height of the stylolite peaks [*Delair and Leroux*, 1978]. Because there could have been contamination by a fluid, this analysis gives only a qualitative estimate of the amount of dissolution.

[14] In the following we assume that fluid circulation is a late event during stylolite formation and that fluids-rock interactions associated with this circulation did not modify the statistical properties of the stylolite surfaces. This assumption is relevant in the sense that we show below that all the stylolites have the same statistical properties, independent of their geological history and geographic origin.

2.2. Statistical Properties of Stylolite Topography

[15] We have determined the scaling behavior of the various stylolites with optical and mechanical profilometers (Table 1 and Figure 4). Topographic height fields (see Figure 5) were measured with two different laser profilometers (one at Rennes University, France, with a horizontal

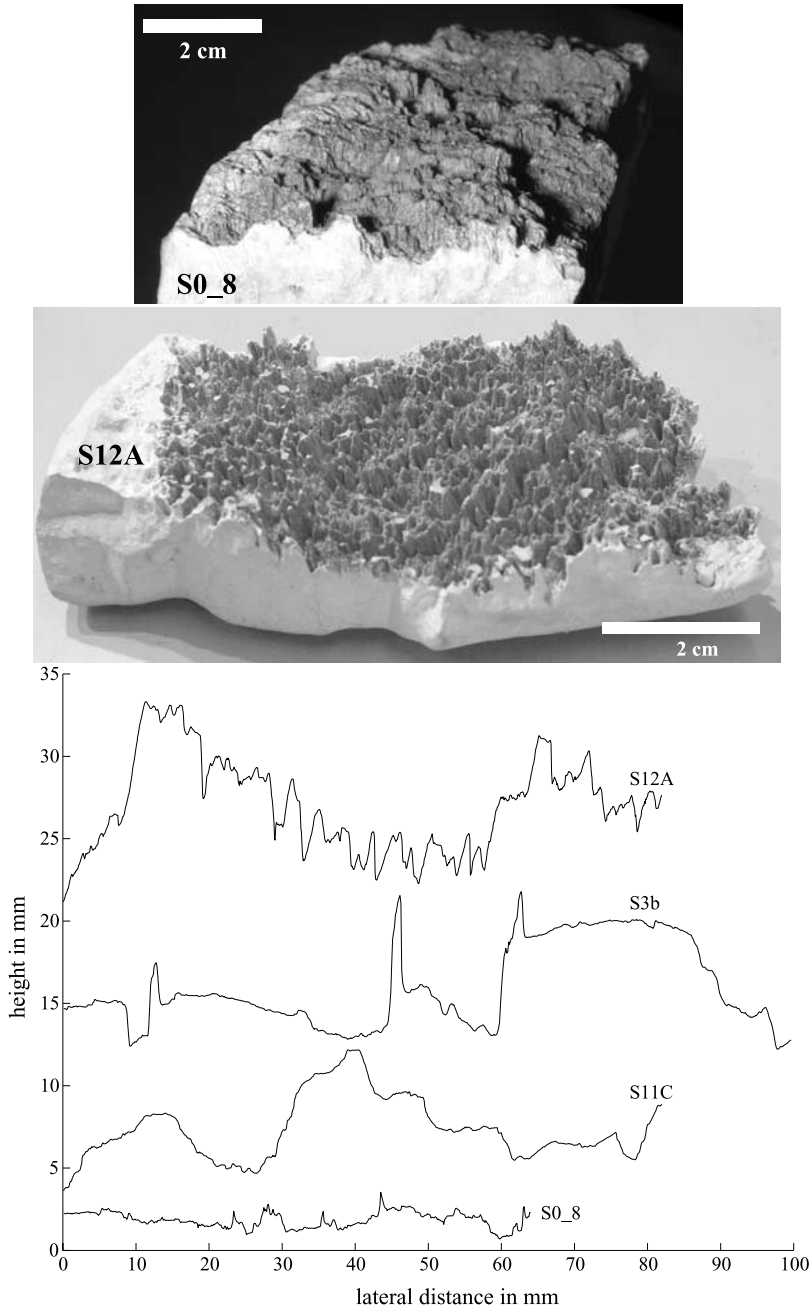

Figure 1. Examples of stylolites at different scales in limestones showing the variety of morphologies and peaks amplitudes. top) Sample S12A, with a roughness of up to 5 millimeters. Sample S0-8 with a roughness of up to 2 millimeters. bottom) Measured profiles of four representative stylolites we have analyzed. These stylolites are ordered according to increasing roughness from bottom to top.

resolution of 125 μm, one at Ecole Normale Supérieure de Paris, France (ENS) with a resolution down to 30 μm) and one mechanical profilometer (ENS) with a resolution of 25 μm. Between 4 and 600 × 600 parallel profilometer transects were conducted on each surface. These profiles are then used to create topographic maps of each surface.

[16] The mechanical profilometer measurements were performed with a sapphire needle with a 25 μm tip radius, which moves up and down and stops when it touches the surface of the stylolite. Between successive measurements, the stylolite surface is displaced laterally according to a prescribed pattern so that the height of the surface can be measured at an array of lateral positions in the plane of the stylolite. The vertical resolution of this device is 3 μm. The time required for a single measurement is approximately 2 seconds, several times longer than for laser measurement. Consequently, we performed only four mechanical profilometer measurements along linear profiles, for the purpose of comparison with laser profilometer data.

[17] The laser measurements were performed by directing a laser beam onto the surface. The distance between the laser and the stylolite is measured via the time of flight of

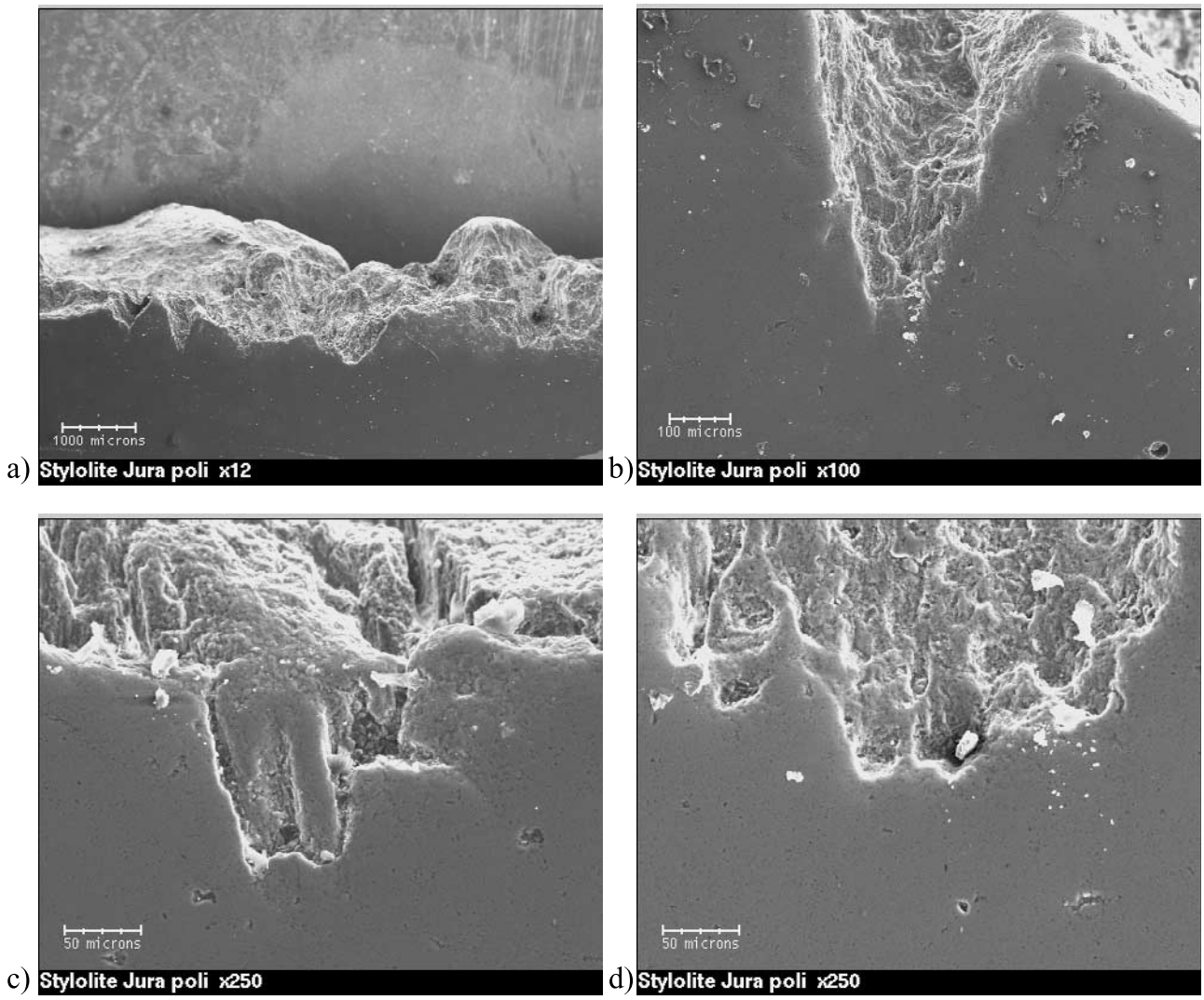

Figure 2. Scanning electron microscope image of a stylolite surface from the Jura area on different scales (sample SJuras1). a) View of the rough surface. b) View of an individual peak on a scale that is about ten times smaller. c–d) Small scale roughness on a scale that is about 20 times smaller than that in part a).

the reflected beam (Rennes University) or by triangulation (ENS). The former has a vertical precision of 30 μm and the latter of 3 μm. The surface height field was constructed by displacing the sample by horizontal increments of 30 to 125 μm along horizontal parallel profiles. Each profile was separated by the same 30 to 125 μm increments. The precision of the horizontal motions is 12 μm for the Rennes instrument and below 1 μm for the ENS instrument.

[18] If a stylolite is approximated by a rough surface that fluctuates spatially about a plane, then the amplitude of the roughness can be defined as the *rms* (root-mean-square) distance between the rough surface and the average plane defined from a least square fit. This quantity characterizes the mean amplitude of the peaks. It might depend on the size of the sampled area and it is defined as

$$A_{rms}(S) = \sqrt{\frac{1}{N}\sum_{i=1}^{N}(z_i - \bar{z})^2}, \qquad (1)$$

where S is the sampled area of the stylolite surface, z_i is the height of the ith point on the area and $\bar{z}$ is the mean height of the surface, which is discretized at N points.

[19] Two types of statistical properties were calculated to characterize the roughness of the stylolites: the *rms* roughness amplitude A_{rms} of each surface for a given sampled area and the roughness exponent (or Hurst exponent) H of the topographic profiles which characterizes the sensitivity of the roughness amplitude with respect to the size of the sampled area: $A_{rms} \propto S^{H/2}$. The Hurst exponent, H, could be determined from the dependence of A_{rms} on S; however, we determined H using the Fourier power spectrum (FS) [*Meakin*, 1998] and the average wavelet coefficient technique (AWC) [*Mehrabi et al.*, 1997; *Simonsen et al.*, 1998; *Hansen et al.*, 2000].

[20] Once the topography of a surface was acquired we carried out a pre-treatment of the raw data before calculating statistical properties of the profiles and the surfaces. The mean plane of each surface was first calculated by two-dimensional mean-squared regression and subtracted from

Table 2. X-Ray Fluorescence Analysis of the Whole Rock and the Content of the Stylolite Interfaces

Stylolite	Sample	Fe_2O_3, %	TiO_2, %	P_20_5, %	CaO, %	SiO_2, %	Al_2O_3, %
S3B	whole rock	0.78	0.07	0.05	83.2	3.89	1.53
S3B	interface	3.33	0.73	0.27	23.7	53.6	9.77
S1sup	whole rock	0.74	0.10	0.06	82.5	8.03	1.41
S1sup	interface	2.05	0.61	0.21	16.5	67.9	7.13
S13A	whole rock	0.46	0.04	0.04	92.6	0.01	0.08
S13A	interface	2.87	0.31	0.23	68.6	18.57	4.81
S11	whole rock	0.61	0.04	0.01	92.1	0	1.17
S11	interface	12.69	0.89	0.12	26.2	39.2	13.13

the initial data. This removes any planar tilt of the surface and sets the mean height to zero.

2.3. Fourier Analysis

[21] The aim is to quantify the scaling behavior and demonstrate that the surface remains unchanged under the transformation $\Delta x \rightarrow \lambda \Delta x$, $\Delta z \rightarrow \lambda^H \Delta z$. The Hurst exponent H can be estimated from the Fourier power spectrum which has a power law form with an exponent of $(-1-2H)$ for a 1-dimensional self-affine profile [*Barabási and Stanley*, 1995; *Meakin*, 1998].

[22] A set of parallel cuts was taken through the digitized surface in a plane perpendicular to the plane of the stylolite to obtain a series of parallel profiles. For each profile, the Fourier power spectrum $P(k)$, i.e., the square of the modulus of the Fourier transform, was calculated as a function of the wave-number k. Then the spectrum of the whole surface was calculated by stacking all the 1D Fourier transforms to reduce the noise associated with individual profiles. For each profile of length L containing N increments, the spatial frequencies range between $1/L$ and the Nyquist frequency $N/2L$ (i.e., the reciprocal of the interval between data points). In this range of frequencies, fall-of problems at short wavelengths are avoided. This method was applied to both the laser and mechanical profilometer data obtained from the same stylolite (Figure 6a). For both data sets, the Fourier analysis give the same results, the only difference is that the mechanical data (4 profiles on the surface Sjuras1) are more noisy than the laser data (up to 1024 profiles on the same surface). These results indicate that the roughness statistics are independent of the measurement device.

[23] The Fourier spectra show that the roughness of the stylolite surfaces can be described in terms of two self-affine regimes. For small wave-numbers k (or large

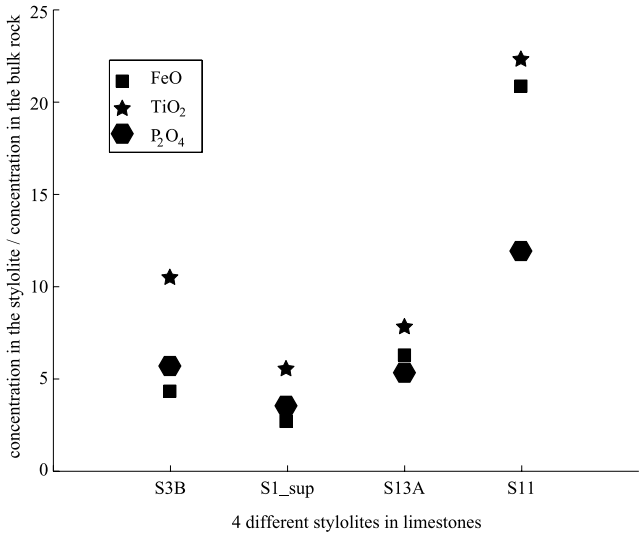

Figure 3. X-ray fluorescence analysis of the bulk rock and the stylolite interface for four different samples.

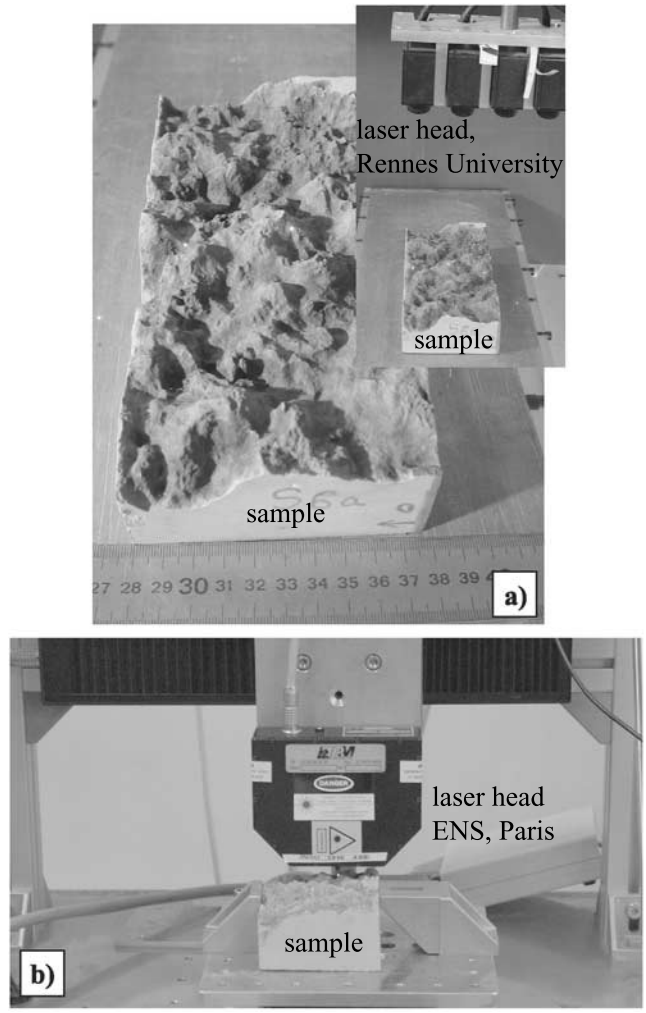

Figure 4. Measurements of the stylolites surfaces with a laser profilometer. Two different lasers were used. One in Rennes University (a), with a step increment of 125 μm (surface S6) and one at the Ecole Normale Supérieure Paris (b), with increments of 30 μm (surface S10A). (See Table 1.)

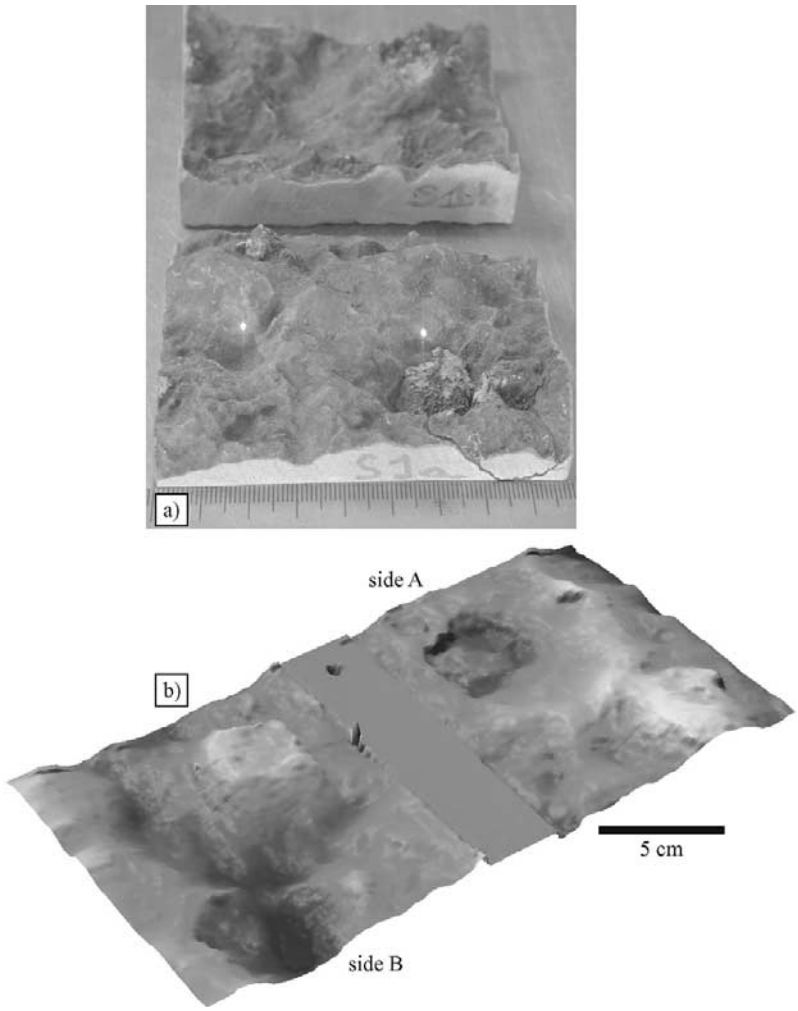

Figure 5. Surface S1-sup measured with a laser (Part a). In Part b, the height field obtained from the laser profilometry is shown. The Fourier and wavelet statistics were performed on such data.

length scales), the slope of the Fourier spectrum scales as k^{-2}, whereas the scaling exponent is -3.2 for large wavenumbers (Figure 6a). A well-defined characteristic wavenumber k^* characterizes the transition between the two regimes. For this example, the characteristic length is close to 1 mm. To summarize, $P(k) \propto k^{-3.2}$ for $k < k^*$, and $P(k) \propto k^{-2}$ for $k > k^*$. This scaling behavior can be related to the Hurst exponent of the surface. A self-affine surface is defined by a single scaling behavior, and $P(k) \propto k^{-(1+2H)}$, where H is the Hurst exponent [*Meakin*, 1998]. This corresponds to $H_1 \approx 0.5$ and $H_2 \approx 1.1$ for small and large wavenumbers respectively. For an asymptotic self-affine fractal the Hurst exponent H lies in the range $0 \leq H \leq 1$. Effective values greater than unity are a consequence of proximity to crossovers and a limited range of scaling. An effective value of 1.1 is consistent with an asymptotic value of unity (a Hurst exponent of 1.0 for an underlying process that is not influenced by other processes).

2.4. Wavelet Analysis

[24] The Fourier analysis results were verified by using an independent method, based on the average wavelet coefficient (AWC) [*Mehrabi et al.*, 1997; *Simonsen et al.*, 1998; *Hansen et al.*, 2000]. This methods consists of wavelet transforming each one-dimensional trace $h(x, y = \text{const})$, where the transform is defined as

$$W_{a,b} = \frac{1}{\sqrt{a}} \int_{-\infty}^{+\infty} dx\ \psi\left(\frac{x-b}{a}\right) |h(x, y = const)|, \qquad (2)$$

where ψ is the wavelet. Then the wavelet coefficients are averaged over the translation factor b for each length scale a.

$$W_a = \langle W_{a,b} \rangle_b. \qquad (3)$$

If the trace is self affine, the wavelet transform verifies statistically for any λ as $W[h(\lambda x)]_{a,b} = \lambda^H W_{a,b}$. Accordingly, the averaged wavelet coefficients scale as

$$W_a \propto a^{H+1/2}. \qquad (4)$$

[25] A wide range of wavelet functions can be used. For a simple and efficient implementation we chose the Daubechies wavelet of order 12 as suggested by *Simonsen et al.* [1998].

[26] The two scaling regimes separated by a well-defined length scale a^* are also revealed using this method (see

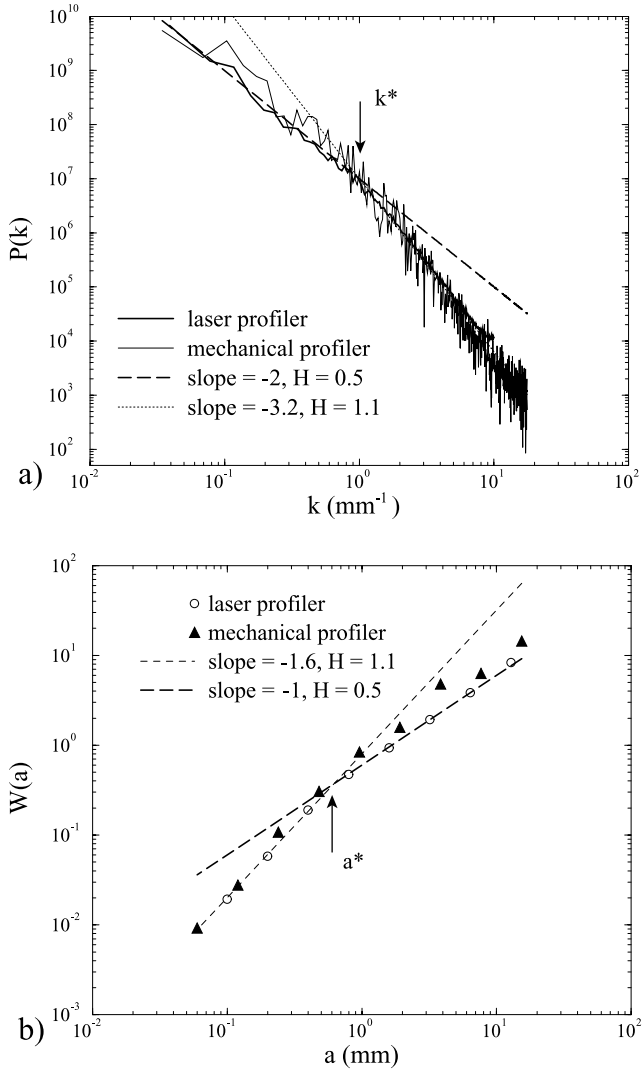

Figure 6. a) Fourier analysis of the surface Sjuras1 measured with a mechanical profilometer and a laser device. b) Wavelet analysis of the same data.

Figure 6b). The values obtained for the Hurst exponents in the two scaling regimes and the crossover length were essentially the same using the data obtained from the laser device and the mechanical profilometer, confirming the results obtained from Fourier analysis.

[27] In addition, we have evaluated the directional morphological isotropy of the stylolites. Two sets of profiles were extracted from the topographic maps along perpendicular directions and the wavelet analysis was performed in these two directions. For all the stylolites, the AWC spectrum in both directions were similar (Figure 7). For a single stylolite surface this test would not be enough to prove the isotropy of a surface, since the axes of the anisotropy, if it exists, could be aligned at an angle of 45° with respect to the directions along which the surface profiles were measured and analyzed. Under these conditions the same results would be obtained for both sets of profiles. However, for all the surfaces that we have measured, the perpendicular directions along which the profiles were measured were chosen randomly, and no anisotropy could be detected. This behavior is common for the population of stylolites that we analyzed providing strong evidence for the isotropy of sedimentary stylolite surfaces.

2.5. A Characteristic Length Scale

[28] The most striking result of this investigation is that the scaling behavior of all the stylolites that we investigated turned out to consist of two regimes, each characterized by a straight line on a log-log scale in Figures 6 and 8, intersecting at a length a^* of 0.18 to a few millimeters.

[29] The crossover length a^* is well defined for each stylolite (Table 1). This parameter can be used to scale the surface roughness and collapse all the data onto a single curve (Figure 8). The crossover is a transition between short and long-scale processes, and the crossover length can be thought of as the point at which dominance by one process given way to dominance by the other. We propose below that on short length scales, with an effective Hurst exponent close to 1.1, capillary effects dominate and at large length scale, with a Hurst exponent close to 0.5, the stylolite geometry is controlled by stress redistribution around the random heterogeneities of the rock.

2.6. Discussion

[30] Usually, the scaling properties of rough surfaces are studied by means of the scale dependent roughness $\delta h(l)$ that measures the height difference between two points of the surface separated by a distance l. The scaling shows up as a functional dependence $\langle \delta h(l) \rangle \propto l^H$, where $\langle \cdots \rangle$ indicates an average over a large number of measurements. H is called the Hurst exponent. This exponent can be obtained by computing the Fourier power spectra $P(k)$ of the profiles along the surface as a function of the wavenumbers $k = 1/l$. The scaling behavior of self-affine profiles is characterized by a power-law dependence $P(k) = k^{-(1+2H)}$ [*Meakin*, 1998]. By using the AWC analysis, the scaling is characterized by a power-law dependence of the spectra

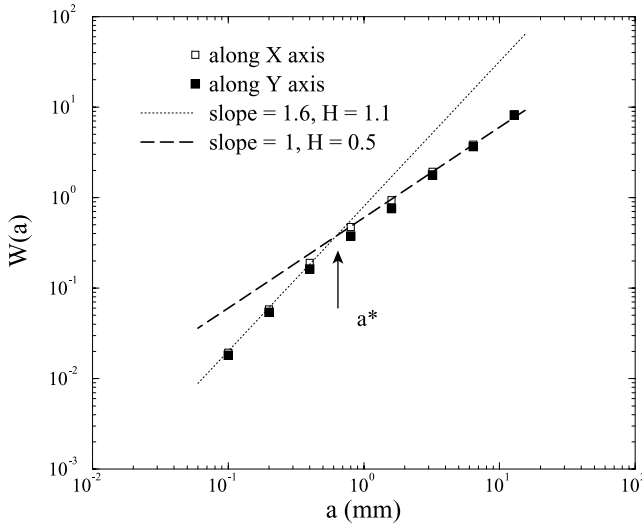

Figure 7. Wavelet spectrum of the stylolite Sjuras1 measured with a laser profilometer. The statistics were calculated for profiles in two directions (two sets of perpendicular cuts through the surface in planes perpendicular to the plane of the stylolite).

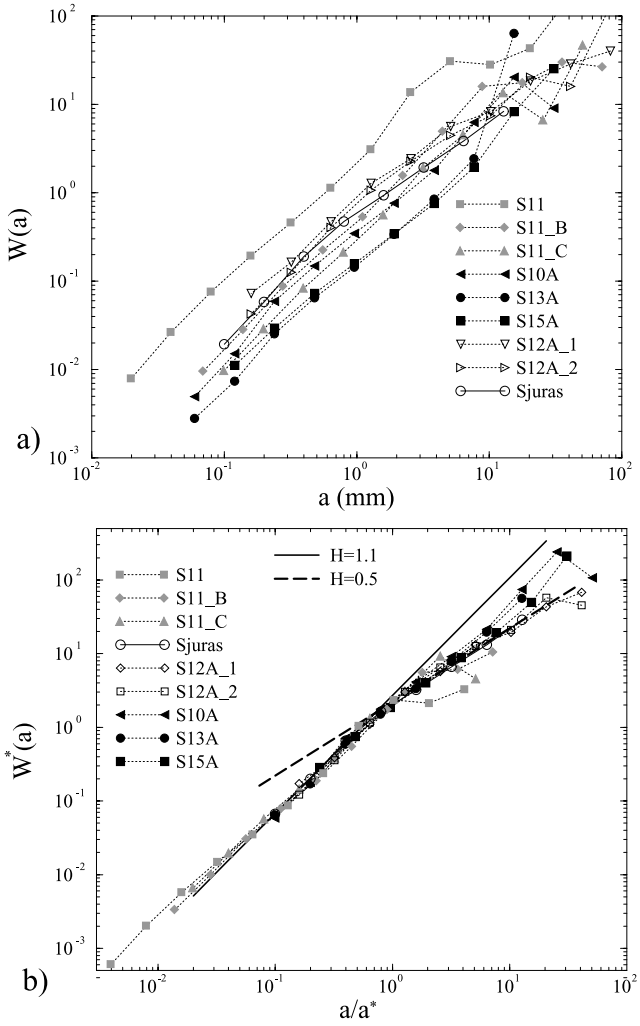

Figure 8. a) Wavelet analysis of all the stylolite surfaces studied. b) A data collapse illustrating that $W(a) = W(a^*)$ $f(a/a^*)$, where $f(x)$ is a scaling function common to all of the stylolites.

$P(k) = k^{H+1/2}$. These two methods are independent, and together they provide a measure of the consistency of the statistical methods used to calculate the Hurst exponent. Our analysis indicates that stylolites are characterized by two self-affine regimes separated by a well-defined characteristic length scale a^*. For small wave-numbers (i.e., large length scales) the Hurst exponent $H_1 \approx 0.5$ and for large wave-numbers (i.e., small length scales), $H_2 \approx 1.1$. The latter value is similar to that obtained for experimental microstylolites by *Gratier et al.* [2004]. All the stylolites that we analyzed showed this universal behavior.

[31] There is other evidence that stylolites have a self-affine fractal structure. For example, *Drumond and Sexton* [1998] measured a Hurst exponent of 0.65 using a cut through a limestone stylolite. The Hurst exponent was determined by using the Fourier power spectrum. Although the power spectrum was quite noisy, it could be represented by a power law, corresponding to $H \approx 0.65$ over almost two wave-number decades corresponding to a two decade range of length scales. On 1D profiles, *Karcz and Scholz* [2003] obtained a Hurst exponent close to 0.55 over 4.5 orders of magnitude for a stylolite from Calcare Massiccio, Italy, and 0.74 and 0.57 for two other lithologies. However, they did not observe a cross-over length-scale.

[32] The values that we obtained for the Hurst exponent are significantly different from the quasi-universal value of about 0.75 measured for fracture surfaces in a wide variety of brittle materials [*Mandelbrot et al.*, 1984; *Power et al.*, 1987; *Maloy*, 1992; *Schmittbuhl et al.*, 1993; *Kim et al.*, 1997] except for that obtained for sandstone fractures [*Boffa et al.*, 1998]. However, it is also clear that stylolite surfaces differ substantially from fractures in brittle materials in having a far greater surface area relative to the area of the flat surface about which the stylolite surfaces fluctuate. This difference can be described through the magnitude of the topothesy, which is defined as the length scale over which the slope of the topography is equal to unity [*Simonsen et al.*, 2000]. Stylolites have a topothesy that is much larger than that of fractures.

[33] A qualitative correlation was observed between the amplitude of the roughness and the characteristic crossover length a^*. In Figure 8, top, the surfaces are sorted according to the amplitude of the peaks: black curves correspond to smooth stylolites, with a low A_{rms} roughness, gray curves correspond to stylolites with well-defined peaks, and dark curves with open symbols are intermediate. The stylolites that have, visually, the highest peaks have a characteristic length a^* of the order of 1–3 mm, whereas 'smooth' stylolites have a characteristic length a^* that is less than 1 mm (Table 1).

3. Modeling Stylolite Surface Growth

[34] A stylolitic surface can be regarded as the current dynamic interface during the mutual pressure solution of two blocks of rock. It is a 2+1-dimensional object that has developed through time. The 2+1-dimensional notation is used for a surface that fluctuates in a third dimension about a two-dimensional plane. Stylolites can be described in terms of the propagation of a growth front that leaves behind a structure that does not change, or the growth of fluctuations about a stationary plane. These two scenarios are equivalent if the propagation of a growth front is described in a coordinate system that moves with the front. We study this development through a phenomenological approach used widely in physics to quantify various rough surface growth processes. We propose a simple 1+1-dimensional model that accounts for capillary and elastic forces and provides some insights into the roughening of an isolated stylolite.

3.1. Driving Forces and Transport Mechanism

[35] Previous works on stylolites indicate that three main ingredients must be included in a realistic model of stylolite formation [*Merino et al.*, 1983; *Ortoleva*, 1994; *Gal et al.*, 1998]: the first is the effect of stress that enhances dissolution in regions of the rock in which the stress is higher; the second is the transport of solutes via a fluid phase; and the third ingredient is a surface smoothing process driven by variation of the curvature related to chemical potential variations along the stylolite surface.

[36] A local increase of stress increases the free energy and also the solubility of the solid. This is the well-known Gibbs effect of stress on free-energy [*Kamb*, 1959; *Weyl*,

1959]. The Gibbs effect is used to explain pressure solution patterns [*Rutter*, 1976]. The relative rates of dissolution of the two solid surfaces drives the interface evolution. This process depends on the relationship between the chemical potential and the energy [*Kassner et al.*, 2001]:

$$\Delta\mu(\mathbf{x}, t) = \Omega(u_e + \gamma\kappa), \tag{5}$$

where $\Delta\mu$ is the local chemical potential difference between the solid and the fluid phase along the interface, Ω is the molecular volume of the dissolving solid, u_e is the elastic energy per unit volume in the solid, γ is the interfacial energy, and κ is the local curvature of the interface. A more complete approach to the mechanical modeling would take into account the full complexity of the normal and tangential stresses effects, including elastic and plastic strain, cataclastic deformation etc. Because of the lack of detailed information and understanding of the complete role played by stress in stylolite formation, we consider that the term u_e, the elastic energy, represents a simplified description of the effects of stress in the model. It is a strong assumption; however, we consider that the long-range elastic distribution of local stress fluctuations can be approximated by this single parameter.

[37] The evolution of the interface is mediated by the diffusion process. Once material has dissolved, solutes are transported in a fluid phase. If the diffusion is in the bulk, the interface velocity v_n is directly proportional to the chemical potential difference: $v_n = m\Delta\mu$ where m is a mobility. In the case of diffusion that is confined to an interface, the interface velocity is given by $v_n = D_i\nabla^2\Delta\mu$, where D_i is an interfacial diffusion coefficient [*Kassner et al.*, 2001]. *Gal et al.* [1998] proposed that in a stylolite diffusion occurs along the solid-fluid interface. However, a study of thin sections of North Sea sandstones indicated that dissolved silica precipitates locally in the bulk rock around the stylolite [*Oelkers et al.*, 1996]. In this case, transport by diffusion occurs in the volume of rock surrounding the stylolite. We assume this second scenario.

[38] *Gal et al.* [1998] have developed a linear stability analysis of stylolite formation. Along the stylolite, the differences in solubility induces heterogeneities in the rates of dissolution. This effect modifies the stress along the surface. The net result of this feedback between stress and dissolution is the amplification of stress heterogeneities and the formation of wavy structures on the dissolving surface. The nonhydrostatically stressed solid can partially release its energy by a morphological instability at the interface [*Müller and Grant*, 1999]. This process is known for homogeneous materials as the Asaro-Tiller-Grinfeld instability (see *Kassner et al.* [2001] for a complete review of the process), and it leads to the amplification of perturbations on an initial noisy surface. When the surface roughness develops, the local curvature varies. This modifies the chemical potential for a given half-space below the stylolitic surface: "bumps" have higher chemical potential whereas "valleys" have a lower chemical potentials. This produces a smoothing of the surface, which competes with the amplification due to stress effects modeled as variations of elastic energy.

3.2. Langevin Model for Stylolite Growth

[39] For many processes in which an initially flat surface or interface evolves into a rough surface, the evolution of the surface can be described by a stochastic differential equation, or Langevin equation, of the form

$$\partial z(\mathbf{x}, t)/\partial t = n(\mathbf{x}, t) + f(z(\mathbf{x}, t)). \tag{6}$$

Here, $z(\mathbf{x}, t)$ is the height of the surface, at lateral position $\mathbf{x}$ (the position along a line in a 1+1-dimensional model or position in a plane in a 2+1-dimensional model) at time t. The height is measured in a moving coordinate system with respect to a plane that is parallel to the initially flat surface.

[40] The term $n(\mathbf{x}, t)$ represents the effects of stochastic processes, which may have a variety of origins. The essence of this equation is that the growth rate $\partial z/\partial t$ at any point depends only on the local properties of the surface and the effects of fluctuations (noise). The function $f(z(\mathbf{x}, t))$ depends on the local slope and curvature of the surface and it describes the physics of the growth process.

[41] In many surface growth equations, the noise is "annealed" noise and this noise drives the evolution of the interface [*Meakin*, 1998]. The simplest model for the noise $n(\mathbf{x}, t)$ is a spatially uncorrelated Gaussian distribution with

$$\langle n(\mathbf{x}, t)\rangle = 0 \tag{7}$$

and

$$\langle n(\mathbf{x}, t)n(\mathbf{x}', t')\rangle = 2\mathcal{D}\delta(\mathbf{x} - \mathbf{x}')\delta(t - t'), \tag{8}$$

where $\mathcal{D}$ is a diffusion coefficient. For this annealed noise the fluctuations $n(\mathbf{x}, t)$ have no time correlations.

[42] In the case of stylolite growth, the dominant contribution to the noise $n(\mathbf{x}, t)$ is directly related to the spatial heterogeneities in the material, which can be considered as local variations of the chemical or mechanical properties of the solid. Under these conditions, the growth equation can be written in the form of equation (6), where $n(\mathbf{x}, z(\mathbf{x}, t))$ is the time independent quenched noise. This quenched noise is not a consequence of the noisy dynamics of the system. Instead, the noise is a consequence of the essentially time independent heterogeneities embedded in the system, and the time dependence of this noise is a consequence of the propagation of the interface through the heterogeneous medium. The addition of material heterogeneities introduces a significant difference from the Asaro-Tiller-Grinfeld instability.

[43] To develop a model for stylolite evolution, we take into account two competing processes: the effects of the stress through the elastic energy, which amplifies perturbations, and the effects of the interfacial energy, which tends to smooth the surface. We shall consider the situation after localization of the strain along an interface. Dissolution is supposed to take place along an existing flat discontinuity. The general equation for surface growth driven by quenched noise (equation (6)) is replaced by

$$\frac{1}{m}\frac{dz}{dt} = \Omega\frac{2(1-\nu^2)}{E}\sigma_0^2\left(1 + \frac{1}{\pi}PV\int_{-\infty}^{\infty}\frac{z(\mathbf{x}') - z(\mathbf{x})}{(\mathbf{x}' - \mathbf{x})^2}d\mathbf{x}'\right) + \Omega\gamma\frac{d^2z}{d\mathbf{x}^2} + \eta(\mathbf{x}, z(\mathbf{x})), \tag{9}$$

where σ_0 is the average effective external stress, which can also take into account the effects of fluid pressure, E is the

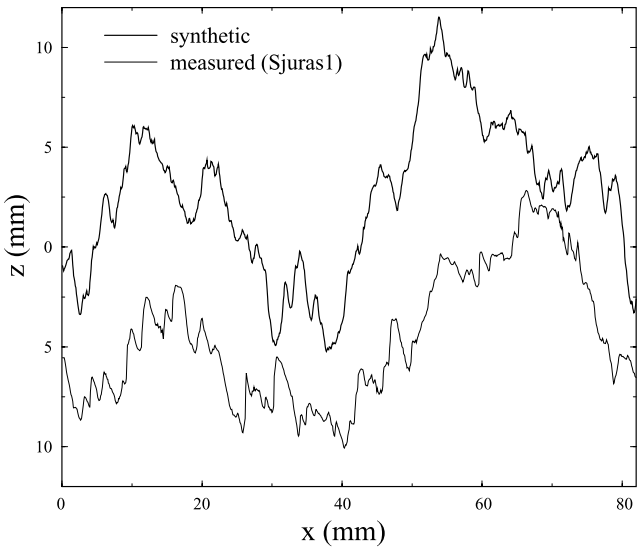

Figure 9. Lower curve: Measured profile in the X direction on the stylolite S12. Upper curve: Result of one simulation according to equation (9).

effective Young's modulus, ν is an effective Poisson coefficient. *PV* stands for the Principal Value. This is the integration between $-\infty$ and $+\infty$ without the contribution at 0, where the integral diverges. Equation (9) includes three driving forces: the long-range elastic interactions, the local capillary effects, which have a stabilizing influence, and the quenched noise fluctuations. The $\Omega\gamma\frac{d^2z}{dx^2}$ term arises because there is a greater density of active zone sites in concave parts of the surface than there are in convex parts of the surface, this accounts for surface tension effects. The non-linear term $\Omega\frac{2(1-\nu^2)}{E}\sigma_0^2(1+\frac{1}{\pi}PV\int_{-\infty}^{\infty}\frac{z(\mathbf{x}')-z(\mathbf{x})}{(\mathbf{x}'-\mathbf{x})^2}d\mathbf{x}')$ arises because the height of the stylolite depends on the stress evaluated over the entire surface. This is a non-local term, which takes into account long-range stress effects. This term can be calculated using the mathematics of Green's functions [*Bilby and Eshelby*, 1968; *Gao and Rice*, 1989].

[44] We have solved numerically equation (9) for the 1+1-dimensional case using an event driven algorithm [*Schmittbuhl et al.*, 1995; *Schmittbuhl and Vilotte*, 1999]. This model consists of a sequence of "growth events" but the number of events is not necessarily linearly related to elapsed time in the physical system. The periodic interface is discretized in 2048 elements. At the start of a simulation, the interface is flat. At each step, the cell that exhibits the maximum speed dz/dt according to equation (9) is located. This cell is then advanced by a random amount dh uniformly sampled from the range [0, 1]. The local fluctuation of the chemical potential $\eta(\mathbf{x}, z(\mathbf{x}))$ is updated from a prescribed distribution chosen to be uniform over the range [0, 1]. In this model the interface always advances into the most unstable cell. After a transient regime, we observed that the width of a rough interface approaches a stationary value. The result is a rough profile that can be compared with that measured on a real stylolite (Figure 9).

[45] The profiles were analyzed and the results were averaged over 500 simulations. A well-defined crossover length, which is controlled by the balance between the magnitude of the elastic and capillary effects separates two self-affine regimes (Figure 10).

3.3. Discussion

[46] As expected, the mechanical regime with an exponent $H_1 \approx 0.4$, is dominant at small wave-numbers (large length scales). At large wave-numbers (small length scales), the capillary regime dominates with an effective Hurst exponent close to $H_2 \approx 1.2$. The Hurst exponents obtained from the model are slightly different from the values obtained by analyzing real stylolites.

[47] This might be explained by the dimension difference: The natural surfaces are 2+1-dimensional interfaces, but the model is 1+1-dimensional. This is a fundamental difference, and in most cases, for most growth models, the characteristic exponents depend on the dimensionality of the growing surface and the dimensionality of the space in which the surface is growing.

[48] The main success of the model is its reproduction of two self-affine scaling regimes separated by a rapid crossover. It gives some physical understanding of the crossover and a possible link with physical parameters.

[49] *Kassner et al.* [2001] performed a linear stability analysis of the competition between mechanical and capillary forces in the case of a stressed solid in equilibrium with its melt and showed that there is a characteristic length scale l_c for which the effects of elastic stress and surface tension cancel. This specific length scale can be extracted from equation (9) and is equal to

$$l_c = E\gamma/2\sigma_0^2(1-\nu^2), \tag{10}$$

where E is the Young's modulus of the solid, σ_0 is the normal stress, γ is the solid-fluid interfacial energy, and ν is the Poisson coefficient of the solid. Typical values for

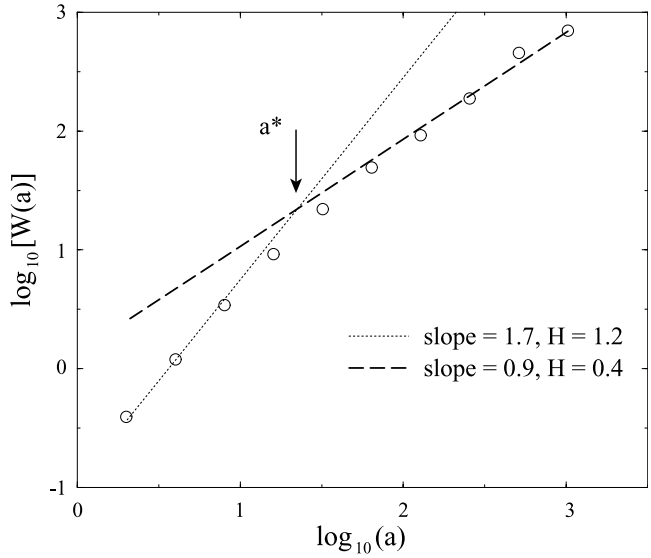

Figure 10. Wavelet analysis of 1D surface roughening according to equation (9). The competition between stress effects and surface tension leads to two scaling regimes. For small wavelengths, $H_1 = 1.2$, whereas for large wavelengths $H_2 = 0.4$.

limestones are $E = 8 \cdot 10^{10}$ N/m^2, $\nu = 0.25$, and $\gamma = 0.27$ J/m^2 for a water-calcite surface. As we obtain $l_c \approx 1$ mm, we can evaluate the required stress: $\sigma_0 \approx 4.8$ *MPa*. This is consistent with the values of differential stresses in the first two kilometers of the crust.

[50] The crossover length scale l_c is controlled by the balance between the elastic forces on the interface and the "capillary" forces. We propose that l_c corresponds to the characteristic length a^* measured on the stylolites. Since l_c depends on the stress σ_0 at which the stylolite developed, it provides a way to estimate the value of a "fossil" stress in the solid. However, the stress effects would have to be integrated with all its complexity to quantify this fossil stress. This is a challenging problem.

[51] On small length scales, the Hurst exponent is close to 1.1. This value is similar that obtained from simulations of quasi-static pinning of fluid interfaces [*Roux and Hansen*, 1994]. In their model, the front of a propagating interface can be pinned by impurities with random strengths. The propagation front is shown to develop a self-affine profile, with an effective Hurst exponent close to 1.2. In their calculations, this exponent is characteristic of a process dominated by capillary effects.

4. Conclusions

[52] We have studied sedimentary stylolites in limestones that can be separated to reveal the delicate three-dimensional geometry of their two sides. Laser and mechanical topographical measurements indicate that stylolite surfaces have two scaling regimes separated by a well-defined characteristic length scale: at small wavelengths, the effective Hurst exponent is equal to 1.1 m, whereas at long wavelengths it is close to 0.5. The crossover between the two scaling behaviors defines the characteristic scale a^* of the surface. We propose that a^* characterizes the competition between two effects: capillary forces that tend to smooth the surface and stress perturbations related to the heterogeneity of the rock that amplify instabilities. We propose that the crossover length a^* provides a measure of a fossil stress along the interface. To proceed further in this analysis would require additional measurements of properties that might influence the growth of stylolites including the grain size, temperature, age, mineral content, porosity, and permeability. The effects of these variables on the crossover length a^* and other aspects of the stylolite morphology would need to be determined. This would be a challenging task because these quantities cannot be independently varied. A combination of physical and geological understanding may lead the idea that one or more of these parameters have a dominant influence on stylolite formation. It would be necessary to study a large number of stylolite surfaces collected from a variety of geological settings to test such an idea.

[53] We have proposed a simple 1+1-dimensional phenomenological model of surface growth based on the two main ingredients of stylolite formation: strain energy and interface energetics. By propagation of a surface under the influence of these two components in a noisy (heterogeneous) solid, we can reproduce the crossover between two scaling behaviors with power-law exponents similar to those measured using stylolites. This is a promising approach, and the next step will be to solve the problem in three-dimensions, i.e., the propagation of a 2+1-dimensional interface in three-dimensional space.

[54] Another characteristics of stylolites is the collective behavior of an ensemble of stylolites in a rock. They tend to anastomose and cut across each other. We did not investigate this problem in this study. However, it poses an additional challenge that must be met to develop a comprehensive understanding of the formation of stylolite patterns.

[55] **Acknowledgments.** P. Meakin, E. Merino, and F. Renard would like to thank the Center for Advanced Studies at the Norwegian Academy of Science and Letters for its support during the early stages of this project. This project was supported by the Centre National de la Recherche Scientifique (ATI and GDR Corinthe to F. Renard) and the French Ministry of Education (ACI to J. Schmittbuhl). We would like to thank C. Pequegnat and D. Tisserand for their technical help. We acknowledge A. Crave, D. Rothman, J. Rice, A. Lobkovsky, B. Evans, M. Bruneton, Y. Bernabé, H. Perfettini, Z. K. Karcz, and B. Goffé for very fruitful discussions, and S. Hickman, A. Revil, and R. Fletcher for helpful reviews.

References

Arthaud, F., and M. Mattauer (1969), Exemples de stylolites d'origine tectonique dans le Languedoc, leur relation avec la tectonique cassante, *Bull. Soc. Geol. Fr.*, *11*, 738–744.

Asaro, R., and W. Tiller (1972), Interface morphology development during stress corrosion cracking: Part 1, Via surface diffusion, *Metall. Trans.*, 1789–1796.

Barabási, A. L., and E. H. Stanley (1995), *Fractal Concepts in Surface Growth*, Cambridge Univ. Press, New York.

Bathurst, R. (1971), *Carbonate Sediments and Their Diagenesis*, Elsevier Sci., New York.

Bayly, B. (1986), A mechanism for development of stylolites, *J. Geol.*, *94*, 431–435.

Bilby, B. A., and J. D. Eshelby (1968), Dislocations and theory of fracture, in *Fracture: An Advanced Treatise*, vol. 1, edited by H. Liebowitz, pp. 99–182, Academic, San Diego, Calif.

Boffa, J., C. Allain, and J.-P. Hulin (1998), Experimental analysis of fracture rugosity in granular and compact rocks, *Eur. Phys. J. Appl. Phys.*, *2*, 281–289.

Carrio-Schaffhauser, E., S. Raynaud, H. Latière, and F. Mazerolles (1990), Propagation and localization of stylolites in limestones, in *Deformation Mechanisms: Rheology and Tectonics*, edited by M. Jones and R. Preston, *Geol. Soc. Spec. Publ.*, *54*, 193–199.

Deelman, J. (1976), Lithification analysis: Experimental observations, *Geol. Rundsch.*, *65*, 1055–1078.

Delair, J., and C. Leroux (1978), Mthode de quantification de la disparition de matire au niveau de stylolites tectoniques et mcanismes de la dformation cassante des calcaires, *Bull. Soc. Geol. Fr.*, *20*, 137–144.

Dewers, T., and P. Ortoleva (1990), A coupled reaction/transport/mechanical model for intergranular pressure solution stylolites, and differential compaction and cementation in clean sandstones, *Geochim. Cosmochim. Acta*, *54*, 1609–1625.

Dickinson, W., and K. Milliken (1995), The diagenetic role of brittle deformation in compaction and pressure solution, Etjo sandstone, Namibia, *J. Geol.*, *103*, 339–347.

Drumond, C. N., and D. Sexton (1998), Fractal structure of stylolites, *J. Sediment. Res.*, *1*, 8–10.

Dunnington, H. (1954), Stylolites development post-date rock induration, *J. Sediment. Petrol.*, *24*, 27–49.

Dunnington, H. (1967), Aspects of diagenesis and shape change in stylolitic limestone reservoirs, in *7th World Petroleum Congress*, vol. 2, pp. 339–352, The Congress, Mexico City.

Fletcher, R. A., and D. D. Pollard (1981), Anticrack model for pressure solution surfaces, *Geology*, *9*, 419–424.

Gal, D., and A. Nur (1998), Elastic strain energy as a control in the evolution of asymmetric pressure-solution contacts, *Geology*, *26*, 663–665.

Gal, D., A. Nur, and E. Aharonov (1998), Stability analysis of a pressure-solution surface, *Geophys. Res. Lett.*, *25*, 1237–1240.

Gao, H., and J. R. Rice (1989), A first-order perturbation analysis of crack trapping by arrays of obstacles, *J. Appl. Mech.*, *56*, 828–836.

Gratier, J.-P., P. Favreau, and F. Renard (2003), Modeling fluid transfer along California faults when integrating pressure solution crack sealing and compaction processes, *J. Geophys. Res.*, *108*(B2), 2104, doi:10.1029/2001JB000380.

Gratier, J., L. Muquet, R. Hassani, and F. Renard (2004), Experimental microstylolites in quartz and modeled application to natural structures, *J. Struct. Geol.*, in press.

Grinfeld, M. (1986), Instability of the separation boundary between a nonhydrostatically stressed solid and a melt, *Sov. Phys. Dokl.*, Engl. Transl., *31*, 831–835.

Guzzetta, G. (1984), Kinematics of stylolite formation and physics of the pressure-solution process, *Tectonophysics*, *101*, 383–394.

Hansen, A., J. Schmittbuhl, G. Batrouni, and F. D. Oliveira (2000), Normal stress distribution of rough surfaces in contact, *Geophys. Res. Lett.*, *27*, 3639–3643.

Heald, M. (1959), Stylolites in sandstones, *J. Geol.*, *63*, 101–114.

Kamb, W. B. (1959), Theory of preferred crystal orientations developed by crystallization under stress, *J. Geophys. Res.*, *67*, 153–170.

Karcz, Z., and C. H. Scholz (2003), The fractal geometry of some stylolites from the Calcare Massiccio Formation, Italy, *J. Struct. Geol.*, *25*, 1301–1316.

Kassner, K., C. Misbah, J. Müller, J. Kappey, and P. Kohlert (2001), Phase-field modeling of stress-induced instabilities, *Phys. Rev. E*, *63*, doi:10.1103/PhysRevE.63.036117. (Available at http://link.aps.org/abstract/PRE/v63/e036117)

Kim, S., Z. H. Yoon, and T. H. Kwon (1997), Scaling behavior of a self-affine fractal interface in a cement fracture experiment, *Phys. A*, *246*, 320–328.

Maloy, K. J. (1992), Experimental measurements of the roughness of brittle cracks, *Phys. Rev. Lett.*, *68*, 213–215.

Mandelbrot, B., D. E. Passoja, and A. J. Paullay (1984), Fractal character of fracture surfaces of metals, *Nature*, *308*, 721–722.

Meakin, P. (1998), *Fractals: Scaling and Growth Far From Equilibrium*, Cambridge Univ. Press, New York.

Mehrabi, A. R., H. Rassamdana, and M. Sahimi (1997), Characterization of long-range correlations in complex distributions and profiles, *Phys. Rev. E*, *56*, 712–722.

Merino, E., and Y. Wang (2001), Geochemical self-organization in rocks: Occurrences, observations, modeling, testing—With emphasis on agate genesis, in *Yearbook Self-Organization*, vol. 11, *Non-equilibrium Processes and Dissipative Structures in Geosciences*, pp. 13–45, Duncker and Humblot, Berlin.

Merino, E., P. Ortoleva, and P. Strickholm (1983), Generation of evenly spaced pressure solution seems during late diagenesis: A kinetics theory, *Contrib. Mineral. Petrol.*, *82*, 360–370.

Müller, J., and M. Grant (1999), Model of surface instabilities induced by stress, *Phys. Rev. Lett.*, *82*, 1736–1739.

Nozieres, P. (1995), The Grinfeld instability of stressed crystals, in *Spatio-Temporal Patterns in Nonequilibrium Complex Systems: NATO Advanced Research Workshop*, vol. 21, edited by P. E. Cladis and P. Palffy-Muhoray, p. 65, Addison-Wesley-Longman, Reading, Mass.

Oelkers, E. H., P. A. Bjørkum, and W. M. Murphy (1996), A petrographic and computational investigation of quartz cementation and porosity reduction in North Sea sandstones, *Am. J. Sci.*, *296*, 420–452.

Ortoleva, P. (1994), *Geochemical self-organization*, Oxford Univ. Press, New York.

Park, W., and E. Schot (1968), Stylolites: Their nature and origin, *J. Sediment. Petrol.*, *38*, 175–191.

Power, W. L., W. B. Durham, S. R. Brown, G. N. Boitnott, and C. H. Scholz (1987), Roughness of natural fault surfaces, *Geophys. Res. Lett.*, *14*, 29–32.

Roux, S., and A. Hansen (1994), Interface roughening and pining, *J. Phys. I*, *4*, 515–538.

Rutter, E. (1976), The kinetics of rock deformation by pressure solution, *Philos. Trans. R. Soc. London, Ser. A*, *283*, 203–219.

Schmittbuhl, J., and J. Vilotte (1999), Interfacial crack front wandering: Influence of correlated quenched noise, *Phys. A*, *270*, 42–56.

Schmittbuhl, J., S. Gentier, and S. Roux (1993), Field-measurements of the roughness of fault surfaces, *Geophys. Res. Lett.*, *20*, 639–641.

Schmittbuhl, J., S. Roux, J. Vilotte, and K. Måløy (1995), Interfacial crack pinning: Effect of non local interactions, *Phys. Rev. Lett.*, *74*, 1787–1790.

Simonsen, I., A. Hansen, and O. M. Nes (1998), Using wavelet transforms for Hurst exponent determination, *Phys. Rev. E*, *58*, 2779–2787.

Simonsen, I., D. Vandembrouck, and S. Roux (2000), Wave scattering for self-affine surfaces, *Phys. Rev. E*, *61*, 5914–5917.

Smith, J. V. (2000), Three-dimensional morphology and connectivity of stylolites hyperactivated during veining, *J. Struct. Geol.*, *22*, 59–64.

Stockdale, P. (1922), Stylolites: Their nature and origin, Ph.D. thesis, Indiana Univ. Stud., Bloomington.

Thomas, R., W. M. Dahl, C. M. Hall, and D. York (1993), Ar^{40}/Ar^{39} analyses of authigenic muscovite, timing of stylolitization, and implications for pressure solution mechanisms—Jurassic norphlet formation, offshore Alabama, *Clays Clay Miner.*, *41*, 269–279.

Weyl, P. (1959), Pressure-solution and the force of crystallization: A phenomenological theory, *J. Geophys. Res.*, *64*, 2001–2025.

J.-P. Gratier and F. Renard, Laboratoire de Géophysique Interne et Tectonophysique, Université Joseph Fourier, BP 53, 38041 Grenoble, France. (gratier@lgit.obs.ujf-grenoble.fr; frenard@lgit.obs.ujf-grenoble.fr)

P. Meakin, Idaho National Engineering and Environmental Laboratory, P.O. Box 1625, Mail Stop 2025, Idaho Falls, ID 83415-2025, USA. (meakp@inel.gov)

E. Merino, Department of Geology, Indiana University, Bloomington, IN 47405, USA. (merino@indiana.edu)

J. Schmittbuhl, Ecole Normale Supérieure, 24 rue Lhomond, 75231 Paris, France. (jean.schmittbuhl@ens.fr)